

# Circumferential Local Ternary Pattern: New and Efficient Feature Descriptors for Anti-Counterfeiting Pattern Identification

Zhaohui Zheng, Bichao Xu<sup>ID</sup>, Jianping Ju, Zhongyuan Guo, Changhui You, Qiang Lei<sup>ID</sup>, and Qiang Zhang

**Abstract**—An important aspect of querying whether a product is likely to be forged is to identify its anti-counterfeiting label. However, the use of image processing technology for label-specific texture analysis to quickly and effectively identify the anti-counterfeiting label has been widely studied. Aiming at the defects of the local binary pattern (LBP) and its variants in texture identification, this paper proposes a new texture model for anti-counterfeiting identification, that is, the circular local ternary pattern (CLTP). The highlight of our technology is that it extracts the effective local texture descriptors by using the random features of inkjet printing. This allows for the technology to not only resist the interference of noise and illumination in images of anti-counterfeiting patterns but also to encode and reorganize the fine linear shape structure. Specifically, this paper extracts the CLTP texture feature in the corresponding key areas and forms the final feature histogram vector for comparison through the one-to-one correspondence between the sample image and the inspected image of anti-counterfeiting pattern. Experiments prove that our method not only has high discrimination, stability and effectiveness but also provides a convenient and practical idea for anti-counterfeiting technology.

**Index Terms**—Circumferential local ternary pattern (CLTP), feature extraction, anti-counterfeiting pattern, key areas.

## I. INTRODUCTION

WITH the rapid development of the economy and the popularity of Internet consumption, the counterfeiting, forgery and piracy of products are rampant. The emergence of low-cost scanning equipment, high-quality printers and good

Manuscript received August 13, 2021; revised October 27, 2021 and February 15, 2022; accepted February 16, 2022. Date of publication February 24, 2022; date of current version March 15, 2022. This work was supported in part by the Science Research Project of Wuhan Institute of Technology under Grant K2021083 and in part by the Program for Innovative Research Team in the Wuhan Railway Vocational College of Technology. The associate editor coordinating the review of this manuscript and approving it for publication was Dr. Alessandro Piva. (*Corresponding author: Bichao Xu.*)

Zhaohui Zheng is with the School of Mathematics and Physics, Wuhan Institute of Technology, Wuhan 430205, China, and also with the Hubei Key Laboratory of Optical Information and Pattern Recognition, Wuhan Institute of Technology, Wuhan 430205, China (e-mail: zhengzhaohui@whu.edu.cn).

Bichao Xu is with the Department of Wuhan Institute of Virology, Chinese Academy of Sciences, Wuhan 430000, China (e-mail: 332429463@qq.com).

Jianping Ju is with the School of Artificial Intelligence, Hubei Business College, Wuhan 430070, China (e-mail: gjdxjpp@whu.edu.cn).

Zhongyuan Guo and Changhui You are with the School of Electronic Information, Wuhan University, Wuhan 430000, China.

Qiang Lei is with the School of Electrical Information Engineering, Wuhan Institute of Technology, Wuhan 430205, China (e-mail: leiqian\_0521@whu.edu.cn).

Qiang Zhang is with the Wuhan Railway Vocational College of Technology, Wuhan 430200, China (e-mail: 382195822@qq.com).

The source code and data: <https://github.com/DoctorZheng/CLTP>  
Digital Object Identifier 10.1109/TIFS.2022.3154289

color copiers makes it easier to counterfeit and forge products, especially in less developed and developing countries. The commonly used anti-counterfeiting method in practice is to add special materials to synthesize anti-counterfeiting patterns [1] as additional security features. However, the costs of these materials are high, and there is a need to rely on human eyes or instruments for identification to achieve high anti-counterfeiting performance, thus, current technology is not sufficiently automated. Therefore, a meaningful research area is digital imaging technology use to identify the textural uniqueness of anti-counterfeiting patterns in spray printing without adding additional security materials. According to the random texture feature introduced by the tiny defects in the mechanical parts and the random diffusion of ink in the printing process, the method ensures the uniqueness of the texture in each printing pattern, which makes the method very useful for the automatic anti-counterfeiting identification of digital images when one item corresponds to another image.

The rapid development of smart phones has made it relatively easy to obtain high-quality digital images. Using digital imaging technology for the anti-counterfeiting identification of digital images is a fast and convenient method with certain reliability. To meet the needs of the public for convenient anti-counterfeiting recognition, we have proposed the statistical difference in key image regions algorithm (SDKR) [2] based on structural difference in our previous research. It uses similar shape features and is easily affected by binarization. In order to ensure the robust extraction of useful texture features under various interference conditions, this paper proposes a novel and robust texture feature extraction method, namely, the circular local ternary pattern (CLTP), which is used to capture the differences of the key details of anti-counterfeiting patterns with strong robustness for the images collected by mobile imaging devices. The main contributions of this paper are as follows:

(i) Based on the analysis of the uniqueness of the anti-counterfeiting texture, we design a new descriptor similar to the LBP: CLTP. The CLTP is more effective for image texture analysis than the traditional LBP and its improved descriptor. It has a stronger identification ability, especially when one item corresponds to one image.

(ii) We introduce the concepts of falling, rising and stable-state structural patterns describing the local fluctuation trend and defining the threshold function.

(iii) We further extend the ternary CLTP to the binary rising pattern (RCLTP) and the binary falling pattern (FCLTP) and combine the statistical histogram into a joint histogram to ensure that the texture description ability should be more robust and stable.

## II. REVIEW OF EXISTING METHODS

Due to the small geometric distortion and noise in the printing process, Gebhardt *et al.* [3] proposed a belonging printing system to distinguish document images by using the difference of the edge roughness, which is used to distinguish laser printing and inkjet printing. However, this method is easily affected by the imaging equipment and ambient illumination, and training data are simultaneously needed. Shang *et al.* [4] proposed using the character edge roughness, noise content and other features for character level identification on three equipment types, and the method achieved an average accuracy of more than 90%. Although the identification type of this method has been extended, it is still affected by illumination. Umadevi *et al.* [5] proposed using the expectation maximization (EM) algorithm to distinguish the type of printer that printed a document. The characters were divided into character areas, background areas and noise areas, and then the printers of the documents were classified by iterative calculation. This method can only be used for basic print type recognition. Akao *et al.* [6] identified the source of an inkjet printer through the distance feature of gear indentation, which is more obvious for paper just printed than for paper that is printed and stored. Elkasrawi and Shafait [7] proposed a method to obtain statistical features from the noise residuals of each character using the unique noise generated by the printer. However, this method is easily affected by the binarization effect when extracting noise. Wu *et al.* [8] proposed a printer model composed of the distance and angle of halftone points and used the Euclidean distance and k-means to identify printer attributes. This method is easily affected by illumination when extracting halftone points, so it is necessary to use a scanner to collect images for recognition. The research on face anti-spoofing attack detection is also of strong reference. Yu *et al.* [9] proposed a novel frame level FAS method based on Central Difference Convolution (CDC), which is able to capture intrinsic detailed patterns via aggregating both intensity and gradient information. And the Central Difference Convolutional Network (CDCN) built with CDC, is able to provide more robust modeling capacity than its counterpart built with vanilla convolution. Parkin *et al.* [10] proposed a new anti-spoofing network architecture that takes advantage of multi-modal image data and aggregates intra-channel features at multiple network layers. They also transfer strong facial features learned for face recognition and show their benefits for detecting spoofing attacks. Although the deep learning method has a good effect on face anti-spoofing attack detection, the one-to-one authenticity identification needs further research.

The texture of an image can sufficiently reflect the internal details. In addition, the texture descriptor and machine learning algorithm can be combined to identify the discrimination pattern, which can be further associated with the uniqueness

of printing. Therefore, the research and development of texture based on identification technology has become a research field of great interest in recent years. Nguyen *et al.* [11] proposed using texture patterns on a microscopic scale to model the micron scanning of printed documents via a binary response model. The parameters of the model depend on the location and shape of points, and the maximum likelihood recognition algorithm is used for authentication. The system needs to use high resolution scanning to obtain micron scanning. Kim and Lee [12] used the halftone mode for laser printer recognition. A set of 15 halftone texture features are extracted by the discrete Fourier transform, and the classifier is trained by a support vector machine. Then, in [13], Kim and Lee used the curvelet transformation and correlation-based attributes to expand the method, but their method is only used for color laser printer recognition. Zhou *et al.* [14] proposed to compute synthetic printer textures from stable small areas within letters. This method classifies 240 characters printed by 12 printers from 10 brands with an average classification accuracy of 96.67%. However, the texture details used in this system cannot be displayed by ordinary scanners without a dedicated, complex and possibly expensive scanning device. Ferreira *et al.* [15] used a multidimensional and multiscale gray level co-occurrence matrix (GLCM) and convolutional texture gradient filter (CTGF) as feature descriptors of documents. In [16], the authors proposed training based on a convolutional neural network (CNN) and selected three different representations for input data: raw data, the median filter residual, the average filter residual. However, they only used the letters "e" and "a" in their papers, letters other than "e" and "a" are not very accurate, and a large number of training pictures need to be prepared in advance. Navarro *et al.* [17] constructed a CTGF map algorithm based on CTGF. This method needs the same scanning method to obtain the document image and can only process the trained characters. Tsai *et al.* [18] combined the discrete wavelet transform (DWT) and gray level co-occurrence matrix (GLCM) to calculate 12 discrete wavelet transform features and 22 gray level co-occurrence matrix features from each corresponding character and used the support vector machine to train and classify the features. In [19], the authors also used a spatial filter, Gabor filter and Wiener filter to calculate more features for classification, but the method only analyzed the scanned images of a laser printer. Sharad *et al.* [20] proposed local texture properties (LTrPs) using a classifier to classify all printed letters. In [21], the authors also introduced a new printer specific local texture descriptor (PSLTD) to capture the texture on a scanned image of printed documents. The dimension of the texture features proposed by Sharad is greatly increased compared with the LBP. This makes the descriptor convenient for subsequent training, but it is not suitable for small sample authenticity identification.

Chen *et al.* [22] proposed an authentication scheme with a mobile imaging device for a 2D barcode. The authentication features include the DFT-based features in frequency domain and the customized LBP-based features in spatial domain. Picard *et al.* [23] presented a system based on integrating copy detection patterns into QR Codes. Li [24] proposed

an image texture calculation method based on the discrete cosine transform (DCT) feature for the identification of anti-counterfeiting label patterns. The calculated DCT feature vector was used as the texture anti-counterfeiting label by combining it with digital anti-counterfeiting technology. Finally, the authenticity of the image was identified by calculating the distance between the texture anti-counterfeiting labels. Zhang [25] evaluated the discrete Fourier transform (DFT), the DCT and the texture feature calculation methods combined with the DFT and DCT and verified the reliability and feasibility of the three methods in the automatic identification algorithm of real anti-counterfeiting labels. In spite of the noise, scaling, rotation and other issues in their experiments, there is no analysis of whether the main factors such as the brightness and contrast ratio affect the identification effect. Although the use of texture classification and recognition has made some good progress, most of the fine texture acquisition methods discussed so far are designed for scanners and special acquisition devices. Therefore, it is still a challenge to choose an appropriate algorithm for the images captured by ordinary mobile devices. For this reason, we have proposed a new texture model for anti-counterfeiting identification. With the purpose is encoding and reorganizing the fine linear shape structure from the images which are captured by ordinary mobile devices.

The structure of the remainder of this paper is as follows: the section III briefly introduces the traditional LBP and its variants, the section IV describes the details of the CLTP feature descriptor proposed herein, and the section V illustrates our anti-counterfeiting pattern identification system. The section VI depicts the comprehensive experimental results and comparative evaluation. The section VII summarizes the paper and proposes some future research directions.

### III. TRADITIONAL LOCAL BINARY PATTERN AND ITS IMPROVEMENT

#### A. Local Binary Pattern

The traditional local binary pattern (LBP) [26] compares the gray value of the central pixel with the gray value of its  $3 \times 3$  square neighborhood and threshold. The obtained value is represented by a binary value (0 or 1), forming an 8-bit binary number and converting it into decimal number. Once the LBP value of each pixel is obtained, a histogram is established to represent the texture image. The LBP descriptor is shown in Fig.1(b). If the gray value of a central pixel in image I is given in a  $3 \times 3$  square neighborhood, the descriptor of operator LBP is defined as follows:

$$f_{LBP}(p_c) = \sum_{i=0}^{M-1} \psi(p_i, p_c) * 2^i \quad (1)$$

where  $p_i$  represents the gray value of the square neighborhood pixels of the center pixel  $p_c$ , and M corresponds to the number of square neighborhood pixels ( $M = 8$ ).  $\psi(\cdot)$  is the unit step function:

$$\psi(x, y) = \begin{cases} 1 & x \geq y \\ 0 & x < y \end{cases} \quad (2)$$

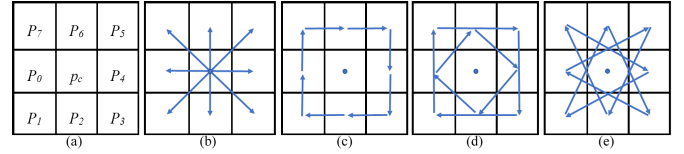


Fig. 1. (a) spatial arrangement of  $3 \times 3$  grayscale templates, (b) layout of LBP descriptors, (c) single loop layout of BGC1, (d) double loop layout of BGC2 and (e) triple loop layout of BGC3.

It is easy to find that the original LBP does not have rotation invariance, for the single comparison size is easy to be affected by noise, and the quantization steps can not reflect the specific gray difference, resulting in the loss of local texture information.

#### B. Binary Gradient Contours

The binary gradient contours BGC1, BGC2 and BGC3 are proposed to reflect the relationship between the neighborhoods of the central pixel [27]. They are pairwise comparisons of the adjacent pixels selected in clockwise order around the  $3 \times 3$  neighborhood of the central pixel by using some predetermined routes. As shown in Fig.1(c-e), the routes of a single loop, double loop and triple loop used by the BGC1, BGC2 and BGC3 descriptors, respectively are shown. The descriptors  $f_{BGC1}(p_c)$ ,  $f_{BGC2}(p_c)$  and  $f_{BGC3}(p_c)$  of the BGC1, BGC2 and BGC3 operators are defined as follows:

$$f_{BGC1}(p_c) = \sum_{i=0}^{M-1} \psi(p_i, p_{(i+1) \bmod M}) * 2^i - 1 \quad (3)$$

$$f_{BGC2}(p_c) = (2^4 - 1) \sum_{i=0}^{\frac{M}{2}-1} \psi(p_{2i}, p_{(2i+2) \bmod M}) * 2^i + \sum_{i=0}^{\frac{M}{2}-1} \psi(p_{2i+1}, p_{(2i+3) \bmod M}) * 2^i - 2^4 \quad (4)$$

$$f_{BGC3}(p_c) = \sum_{i=0}^{M-1} \psi(p_{3i}, p_{3(i+1) \bmod M}) * 2^i - 1 \quad (5)$$

#### C. Local Ternary Pattern

A binary gradient contour is forced to distinguish between binary values for the texture with no significant difference, thus not meeting the requirements of the real texture. Therefore, the local ternary pattern (LTP) [28] solves the above problem by dividing the gray difference into three levels using the width area. For the unit step function of LBP  $\psi(\cdot)$ , the LTP modified the pattern as follows:

$$\psi(x, y) = \begin{cases} 1 & x - y \geq T \\ 0 & |x - y| < T \\ -1 & x - y \leq -T \end{cases} \quad (6)$$

where the threshold T controls the transition width to distinguish three levels. The LTP ensures that the change of the gray value can be ignored in a certain range.

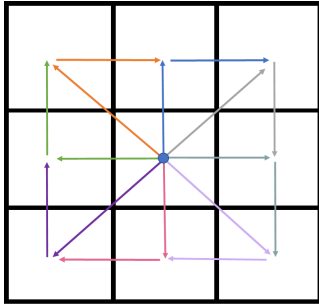


Fig. 2. The layout structure of the CLTP descriptor.

#### IV. CIRCUMFERENTIAL LOCAL TERNARY PATTERN TEXTURE DESCRIPTOR (CLTP)

Inspired by the above operators and considering that the ink unevenness or divergence on the printed page of an anti-counterfeiting pattern is the unique attribute of a printer, this paper proposes a circumferential local ternary pattern (CLTP) with structural difference to improve the recognition ability of the local texture feature.

##### A. Circumferential Ternary Structure

The LBP operator completely ignores the difference of the neighborhood pixels around the center pixel because it is based on the binary comparison between the center pixel and a neighborhood pixel. While the BGC1 operator is based on the binary pixel comparison of the adjacent elements in the neighborhood of the central pixel, it completely ignores the center pixel with discrimination information. The proposed method is based on the comparison between the center pixel and the adjacent elements in the square neighborhood, ensuring that both the center pixel and the neighborhood pixel can be considered, improving the robustness, discrimination and applicability of the texture feature extraction operator. As shown in Fig.2, each path in the  $3 \times 3$  window in the image is composed of a central pixel and two adjacent elements in its neighborhood in a clockwise order. Therefore, each window has 8 paths in total, so the pixel set in the path is defined as  $\{[p_c, p_i, p_{i-1}], \forall i \in [1, 7], (i = 0 -> i - 1 = 7)\}$ , and the corresponding pixel group of each path is  $[p_c, p_7, p_6], [p_c, p_6, p_5], [p_c, p_5, p_4], [p_c, p_4, p_3], [p_c, p_3, p_2], [p_c, p_2, p_1], [p_c, p_1, p_0], [p_c, p_0, p_7]$ .

The difference of the gray values of the pixels measured by the binary value is easily affected by noise, and the difference of similar gray values is forced to be distinguished; therefore, this does not meet the requirements of real anti-counterfeiting pattern textures. Therefore, this paper adopts the ternary value pattern (see equations (6)) to handle the difference of similar gray values  $\psi(p_{i-1}, p_i)$ .

We conducted ablation study for better illustrating the strong competitiveness of CLTP. Table I shows the maximum number of models that can be represented by each operator. LBP and BGC can describe  $2^8$  models, but their focus is different. LTP can describe  $3^8$  models with better performance than LBP and BGC, and can greatly reduce the impact of noise. CLTP can describe  $3^{16}$  models, which considers the

TABLE I  
THE MODEL NUMBER OF TEXTURE OPERATOR

Texture Operator	The number of model
LBP	$2^8$
BGC1	$2^8$
BGC2	$2^8$
BGC3	$2^8$
LTP	$3^8$
CLTP	$3^{16}$

difference between central pixels and neighborhood pixels, and better describes the subtle texture features in authenticity identification. In order to reduce the dimension of CLTP and the influence of external factors (such as illumination, contrast, etc), we will use the microstructure with falling, rising and stable state to represent the local change characteristics of the image.

##### B. The Microstructure With Falling, Rising and Stable State

This paper defines three types of structures, falling, rising and stable states, for the comparison between three pixels and to accurately describe the local fluctuation trend of an image. Let  $[p_c, p_{i-1}, p_i]$  be a set of triples in an image. If the pixel  $p_i$  satisfies the conditions:  $(\psi(p_{i-1}, p_i) = 1 \text{ and } \psi(p_i, p_c) = 1)$ ,  $(\psi(p_{i-1}, p_i) = 1 \text{ and } \psi(p_i, p_c) = 0)$  or  $(\psi(p_{i-1}, p_i) = 0 \text{ and } \psi(p_i, p_c) = 1)$ , then the triple  $[p_c, p_{i-1}, p_i]$  is a rising structure. If the pixel satisfies the conditions  $(\psi(p_{i-1}, p_i) = -1 \text{ and } \psi(p_i, p_c) = -1)$ ,  $(\psi(p_{i-1}, p_i) = -1 \text{ and } \psi(p_i, p_c) = 0)$  or  $(\psi(p_{i-1}, p_i) = 0 \text{ and } \psi(p_i, p_c) = -1)$ , then the triple  $[p_c, p_{i-1}, p_i]$  is a falling structure. If the pixel satisfies the conditions  $(\psi(p_{i-1}, p_i) = 0 \text{ and } \psi(p_i, p_c) = 0)$ ,  $(\psi(p_{i-1}, p_i) = 1 \text{ and } \psi(p_i, p_c) = -1)$  or  $(\psi(p_{i-1}, p_i) = -1 \text{ and } \psi(p_i, p_c) = 1)$ , then the triple  $[p_c, p_{i-1}, p_i]$  is a stable structure. Fig.3 displays the images of the ternary structure of rising, falling and stable states.

The ternary threshold function  $v(\cdot)$  of rising, falling and stable states is defined based on the concepts of falling, rising and stable structures as follows:

$$\begin{aligned}
 v(p_c, p_{i-1}, p_i) &= \psi(p_{i-1}, p_i) \oplus \psi(p_i, p_c) \\
 &= \begin{cases} 1 & p_{i-1} - p_i \geq T \\ 0 & |p_{i-1} - p_i| < T \\ -1 & p_{i-1} - p_i \leq -T \end{cases} \oplus \begin{cases} 1 & p_i - p_c \geq T \\ 0 & |p_i - p_c| < T \\ -1 & p_i - p_c \leq -T \end{cases} \\
 &= \begin{cases} 1 & \psi(p_{i-1}, p_i) + \psi(p_i, p_c) > 0 \\ 0 & \psi(p_{i-1}, p_i) + \psi(p_i, p_c) = 0 \\ -1 & \psi(p_{i-1}, p_i) + \psi(p_i, p_c) < 0 \end{cases} \quad (7)
 \end{aligned}$$

where the threshold  $T$  is set according to the experience value and the degree of recognition of the gray level (In order to improve the degree of recognition, this paper sets  $T=2$ ). When  $v(\cdot) = 1$ , it is a rising structure, when  $v(\cdot) = -1$ , it is a falling structure, and when  $v(\cdot) = 0$ , it is a stable structure.

Fig.4 depicts the calculation of the eigenvalues of the LBP, BGC1, BGC2, BGC3, LTP and CLTP operators on three different sub images (a), (b) and (c). The results of LBP, BGC1,

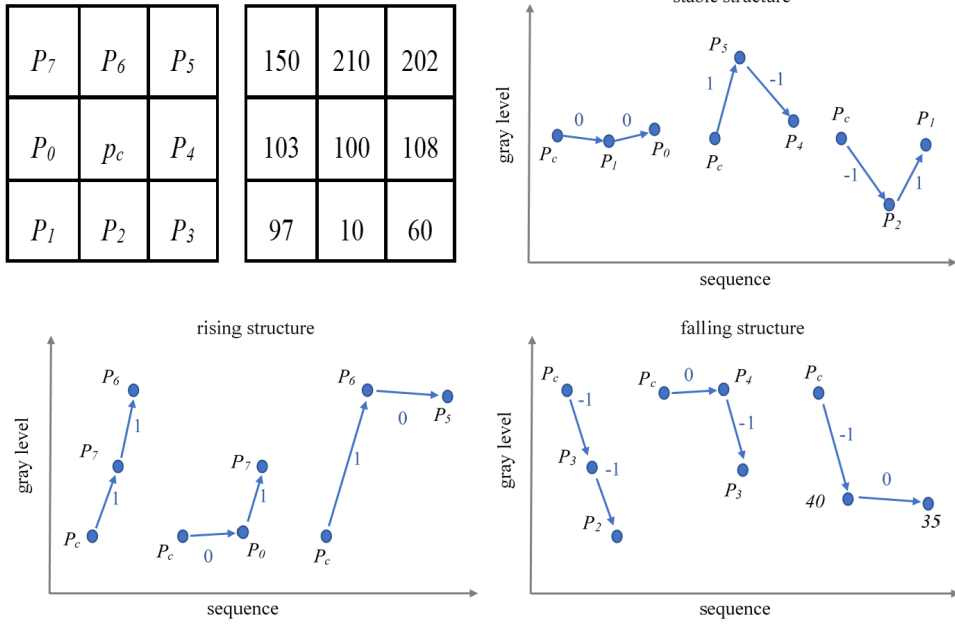


Fig. 3. The corresponding ternary structures of falling, rising and stable states in the  $3 \times 3$  gray level sub-image.

BGC2 and BGC3 in images (a) and (b) are the same, and their differences cannot be distinguished. Although the LTP can distinguish images (a) and (b), the results in images (b) and (c) are the same. However, the CLTP operator introduced in this paper can well distinguish images (a), (b) and (c).

We can replace  $-1$  of the initial CLTP value with  $2$  to ensure the rotation invariance of the CLTP. Then, we rotate the circle neighborhood continuously to get a series of CLTP values and take the minimum value as the CLTP value of the neighborhood. A multiscale problem can be realized by the size of radius and the number of sampling points in the neighborhood. Because the CLTP in this paper mainly aims at identifying anti-counterfeiting patterns, simple preprocessing, such as illumination adjustment, registration, etc., will be conducted in the collection stage of anti-counterfeiting patters; therefore, it is not necessary to consider rotation and multiscale problems.

### C. Rising and Falling Features

Each ternary pattern of the CLTP is divided into the eigenvalues of the rising pattern RCLTP and falling pattern FCLTP to fully display the texture fluctuation and express it in simple binary form. The corresponding ternary threshold function  $v(\cdot)$  can be divided into binary threshold functions  $rv(\cdot)$  and  $dv(\cdot)$ , as is shown in Fig.5. Then, they are regarded as two independent channels of the CLTP descriptor, their respective histograms and similarity measures (L2 norm distance) are calculated, and finally the scores of the two similarities are fused by using simple union rules. The functions  $rv(\cdot)$  and  $dv(\cdot)$  are defined as follows:

$$rv(p_c, p_{i-1}, p_i) = \begin{cases} 1 & v(p_c, p_{i-1}, p_i) = 1 \\ 0 & v(p_c, p_{i-1}, p_i) \leq 0 \end{cases} \quad (8)$$

$$dv(p_c, p_{i-1}, p_i) = \begin{cases} 1 & v(p_c, p_{i-1}, p_i) = -1 \\ 0 & v(p_c, p_{i-1}, p_i) \geq 0 \end{cases} \quad (9)$$

The rotation and scaling problem does not need to be considered as the registration correction has been done before the texture feature extraction of the anti-counterfeiting pattern. Therefore, the two descriptors  $f_{RCLTP}(p_c)$  and  $f_{FCLTP}(p_c)$  decomposed by the CLTP operator are directly obtained by using the kernel functions  $rv(\cdot)$  and  $dv(\cdot)$ .

$$f_{RCLTP}(p_c) = \sum_{i=0}^{M-1} rv(p_c, p_{i-1}, p_i) * 2^i \quad (10)$$

$$f_{FCLTP}(p_c) = \sum_{i=0}^{M-1} dv(p_c, p_{i-1}, p_i) * 2^i \quad (11)$$

We compute the histograms of the RCLTP and FCLTP descriptors separately, and the histograms of the RCLTP and FCLTP descriptors are combined to form the histograms of the CLTP descriptors. This hybrid texture description model has a better texture analysis ability than the single descriptor model.

$$h_{CLTP} = h_{RCLTP} \cup h_{FCLTP} \quad (12)$$

### V. THE APPLICATION OF CLTP IN ANTI-COUNTERFEITING PATTERN IDENTIFICATION

To improve the identification of textures and increase the details for anti-counterfeiting, we designed a type of anti-counterfeiting pattern with a large number of fine and dense random textures according to the randomness of printer ink diffusion on paper. The pattern is a binary anti-counterfeiting pattern with a random fine texture that is generated using a random generation function and fractal

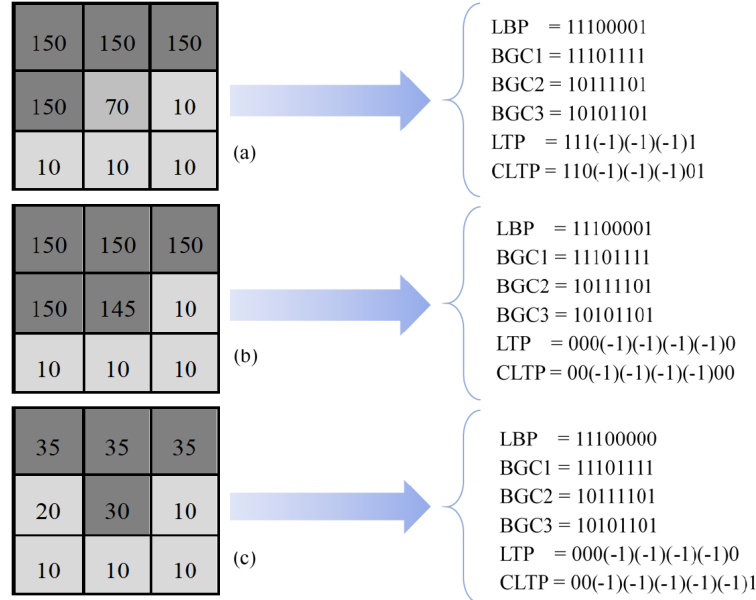


Fig. 4. Eigenvalues corresponding to the LBP, BGC1, BGC2, BGC3, LTP and CLTP operators in the three sub images.

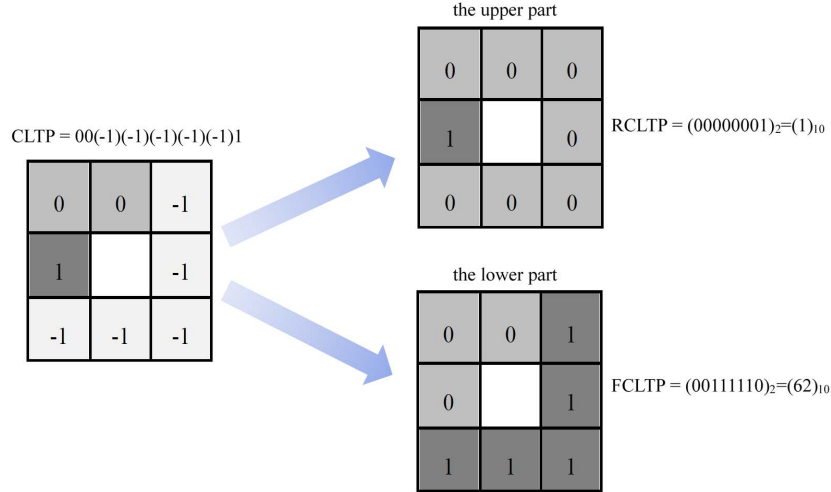


Fig. 5. Two independent channels corresponding to the ternary pattern of the CLTP descriptor.

interpolation method. The shape of the pattern is composed of arbitrary curved thin lines or dots. Each anti-counterfeiting pattern is different and unique with the feature of one object corresponding to one code, thereby increasing the forgery costs to the greatest extent and ensuring the reliability of one-to-one anti-counterfeiting pattern identification. The anti-counterfeiting pattern can be combined with other identification maps simultaneously, as shown in Fig.6. Three concepts are explained as follows for better understanding: anti-counterfeiting pattern is generated by a computer and is copied or printed by printer. Anti-counterfeiting image is the image of the anti-counterfeiting pattern which is collected by a camera. The anti-counterfeiting key area is the area with high anti-counterfeiting performance in the anti-counterfeiting pattern.

#### A. Alignment of Anti-Counterfeiting Image

The matching algorithm [29], [30] is used for preprocessing before the identification of the anti-counterfeiting pattern,

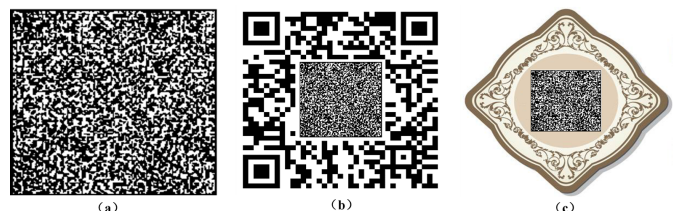


Fig. 6. Anti-counterfeiting pattern and combination anti-counterfeiting patterns. Image a is the original anti-counterfeiting pattern, image b is the anti-counterfeiting pattern in a QR code, and image c is the anti-counterfeiting pattern in a label icon.

and the inspected anti-counterfeiting image is registered and corrected to ensure that the sample image is aligned with the inspected image.

This paper uses the feature matching method to align the anti-counterfeiting images. First, we extract the OBR feature points of the sample image and the inspected image, then



Fig. 7. Anti-counterfeiting image matching process. Image a is the initial match, image b is the matching result after eliminating mismatches, and image c is the positioning result of anti-counterfeiting image.

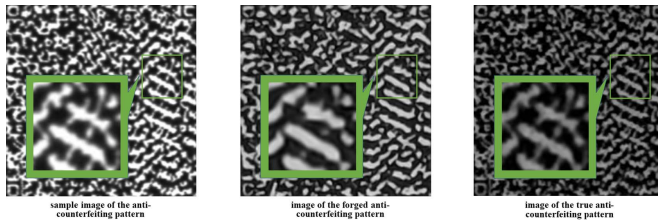


Fig. 8. Contrast map of the difference area between the sample image and the inspected image.

match and filtrate the features in two images using the Brute Force algorithm and FUGC's [29] local linear transformation and obtain the perspective transformation matrix (homographic matrix) to correct the inspected image. Because the acquisition program of the mobile terminal will carry out preliminary alignment of acquisition frame to ensure there will not produce large geometric distortion of the anti-counterfeiting image in the acquisition frame, thereby ensuring the consistency of registration. As shown in Fig.7:

### B. Extraction of Anti-Counterfeiting Key Point Area

Not all areas in the anti-counterfeiting pattern have high anti-counterfeiting performance. For high-precision forgery technology, the local areas with high anti-counterfeiting performance are more important for anti-counterfeiting than other areas, as shown in Fig.8. The areas with high anti-counterfeiting performance are usually corner points, inflection points or small graphic areas with significant features, which can remove a large amount of redundant information in the anti-counterfeiting pattern and focus on the geometric features of the important key areas of the anti-counterfeiting pattern. We use the SUSAN algorithm [31] with a fast calculation speed and strong antinoise ability for the extraction of key points.

After the SUSAN corner points are extracted, a rectangular area with radius R is constructed based on each corner point as the center for subsequent texture feature extraction (In this paper, R=4). The area extraction steps of anti-counterfeiting key points are shown in Fig.8.

### C. Similarity Measurement Based on Distance Transformation

The CLTP is used to conduct feature extraction for each anti-counterfeiting key area image in the given anti-counterfeiting pattern, and the RCLTP and FCLTP are extracted from each pixel in each area image. Then, the

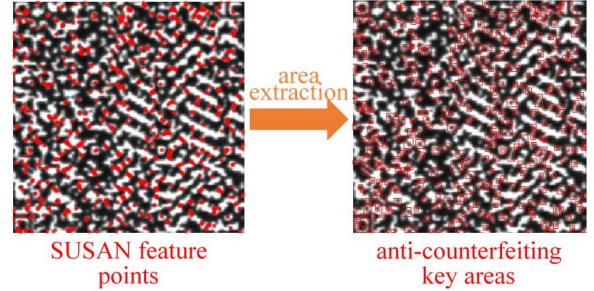


Fig. 9. Area extraction steps of anti-counterfeiting key points.

probability distribution is represented by establishing the statistical histogram of the RCLTP and FCLTP feature images. The histogram  $h_{RCLTP}(\zeta)$  and  $h_{FCLTP}(\zeta)$  are calculated as follows:

$$h_{RCLTP}(\zeta) = \sum_{j=0}^L \delta(f_{RCLTP}(j), \zeta) \quad (13)$$

$$h_{FCLTP}(\zeta) = \sum_{j=0}^L \delta(f_{FCLTP}(j), \zeta) \quad (14)$$

where  $\zeta \in [0, N_{bin}]$ ,  $N_{bin} = 2^8 - 1$  is the number of histogram elements, and L is the number of pixels in an anti-counterfeiting key area image. The function  $\delta(\cdot)$  is defined as follows:

$$\delta(x, y) = \begin{cases} 1 & x = y \\ 0 & x \neq y \end{cases} \quad (15)$$

The similarity between the statistical histogram of the inspected anti-counterfeiting image and the sample anti-counterfeiting image is calculated by the L2 norm distance. Then, the distance formula of an anti-counterfeiting key area image is as follows:

$$d_R(h_{RCLTP}^1, h_{RCLTP}^2) = \sqrt{\sum_{i=0}^{N_{bin}} (h_{RCLTP}^1(i) - h_{RCLTP}^2(i))^2} \quad (16)$$

$$d_F(h_{FCLTP}^1, h_{FCLTP}^2) = \sqrt{\sum_{i=0}^{N_{bin}} (h_{FCLTP}^1(i) - h_{FCLTP}^2(i))^2} \quad (17)$$

where  $h_{RCLTP}^1$  and  $h_{FCLTP}^1$  are the key area image statistical histograms of the inspected anti-counterfeiting pattern,  $h_{RCLTP}^2$  and  $h_{FCLTP}^2$  are the key area image statistical histograms of the sample anti-counterfeiting pattern.

Finally, the distances  $d_R$  and  $d_F$  of all anti-counterfeiting key area images are combined to form the distance feature vector  $v_{dR}$  and  $v_{dF}$ , and the distance scores of the RCLTP and FCLTP features are fused by using simple union rules.

$$v_{dR} = [d_R(1), d_R(2), \dots, d_R(K)] \quad (18)$$

$$v_{dF} = [d_F(1), d_F(2), \dots, d_F(K)] \quad (19)$$

$$[v_{dR}, v_{dF}] = [d_R(1), d_R(2), \dots, d_R(K),$$

$$d_F(1), d_F(2), \dots, d_F(K)] \quad (20)$$

where  $K$  is the number of anti-counterfeiting key areas in an anti-counterfeiting pattern.

Fig.10 demonstrates the overall flowchart of the proposed method that combines the advantages of the LBP, BGC1 and LTP operators to construct robust and informative CLTP texture features, improving the degree of recognition despite complex environmental impacts and small differences. Furthermore, the preprocessing steps of key point area extraction are used to quickly locate possible texture difference areas, greatly improving the real-time performance and robustness of the algorithm. These factors contribute to the overall system performance and robustness.

For intuitive judgment, we usually normalize the statistical histograms  $h_{RCLTP}(\zeta)$  and  $h_{FCCLTP}(\zeta)$ , and then the distances  $d_R$  and  $d_F$  are binarized by the threshold function.

$$d_R(i) = \begin{cases} 1 & d_R(i) > \sigma \\ 0 & d_R(i) \leq \sigma \end{cases} \quad i = 1 \dots K \quad (21)$$

$$d_F(i) = \begin{cases} 1 & d_F(i) > \sigma \\ 0 & d_F(i) \leq \sigma \end{cases} \quad i = 1 \dots K \quad (22)$$

where  $\sigma$  is the threshold value. When the distance is greater than  $\sigma$ , the region is considered dissimilar, otherwise it is similar.  $\sigma$  can be tested by selecting part of data sets to obtain the best classification threshold. In this paper,  $\sigma = 0.32$ .

Finally, we use the threshold function to judge the distance score  $[vd_R, vd_F]$  of RCLTP and DCLTP features:

$$result = \begin{cases} 1 & \left( \sum_{i=0}^K (d_F(i) + d_R(i)) \right) / 2K < \mu \\ 0 & \left( \sum_{i=0}^K (d_F(i) + d_R(i)) \right) / 2K \geq \mu \end{cases} \quad (23)$$

where  $\mu$  is the threshold value. When the distance score is smaller than  $\mu$ , it indicates that the number of dissimilar areas meets the requirements and is genuine. Otherwise, it is forged.  $\mu$  can be tested by selecting part of data sets to obtain the best classification threshold. In this paper,  $\mu = 0.09$ .

## VI. EXPERIMENTAL RESULTS AND ANALYSIS

In this section, we will introduce the experiments used to verify the proposed method. The experiments are conducted on a newly created dataset on which all presented methods are tested and evaluated.

### A. Data Sets and Experimental Settings

The parameters of the algorithm are consistent throughout the experimental process used to verify the performance of the algorithm designed in this paper. These experiments were carried out on a laptop with a 1.8 GHz i7 Intel Core CPU, 16 GB of memory and the Windows 10 operating system with the MATLAB R2016a program installed.

At present, there are few one-to-one anti-counterfeiting research literatures [22], so we use our self-built anti-counterfeiting pattern data set in the early stage [2]. First,

TABLE II  
THE PRINTERS USED IN THE EXPERIMENT

Printer brand	Printer model	Dots Per Inch(dpi)	Printing type
HP	M281fdw	600*600	LaserJet
HP	M436n	600*600	LaserJet
HP	M1136	600*600	LaserJet
HP	P1106	600*600	LaserJet
HP	DJ5078	1200*1200	Inkjet
Canon	MF525dw	600*600	LaserJet
Canon	E568	4800*1200	Inkjet
EPSON	L3118	5760*1440	Inkjet
SAMSUNG	C480W	600*600	LaserJet
Lenovo	M7268W	600*600	LaserJet

TABLE III  
THE MOBILE PHONES USED IN THE EXPERIMENT

Mobile phone brand	Mobile phone model	Physical pixel
APPLE	6s	12 million
APPLE	6s Plus	12 million
APPLE	7	12 million
APPLE	8 Plus	12 million
HUAWEI	Mate 20 Pro	40 million
HUAWEI	Honor20	48 million
OPPO	K1	16 million
VIVO	IQOO	12 million
MI	Redmi Note7	48 million
MEIZU	16	20 million

we use the inkjet printing equipment of the system to print the 20 different samples of anti-counterfeiting patterns and use camera to collect the sample images of the 20 different samples of anti-counterfeiting patterns, then use 10 different brands of laser/inkjet copy printers(see Table II) to print or copy these anti-counterfeiting samples as forged anti-counterfeiting patterns. So there are 20 groups of anti-counterfeiting patterns, and each group has 1 sample of real anti-counterfeiting pattern and 10 forged anti-counterfeiting patterns. Finally, 10 different brands of mobile phones(see Table III) were used to take photos of 20 groups of anti-counterfeiting pattern. Therefore, the data set consists of 20 groups of data, each of which has 1 sample image, 10 real anti-counterfeiting images and 100 forged anti-counterfeiting images.

### B. Experimental Results

This paper tests and compares the CLTP with the most commonly used and most advanced texture features of the GLCM, WDT, LBP, BGC1, LTP, LBPCoHDLBP [32], MRELBP [33], RALBGC [34] to verify the precision of the abovementioned anti-counterfeiting pattern identification method based on CLTP texture features. At the same time, we add the statistical difference in key image regions algorithm(SDKR) [2] based on structural difference in our previous research. This paper utilizes the same preprocessing to ensure the fairness of the evaluation of the texture descriptors, namely, anti-counterfeiting pattern registration. This obtains the corrected

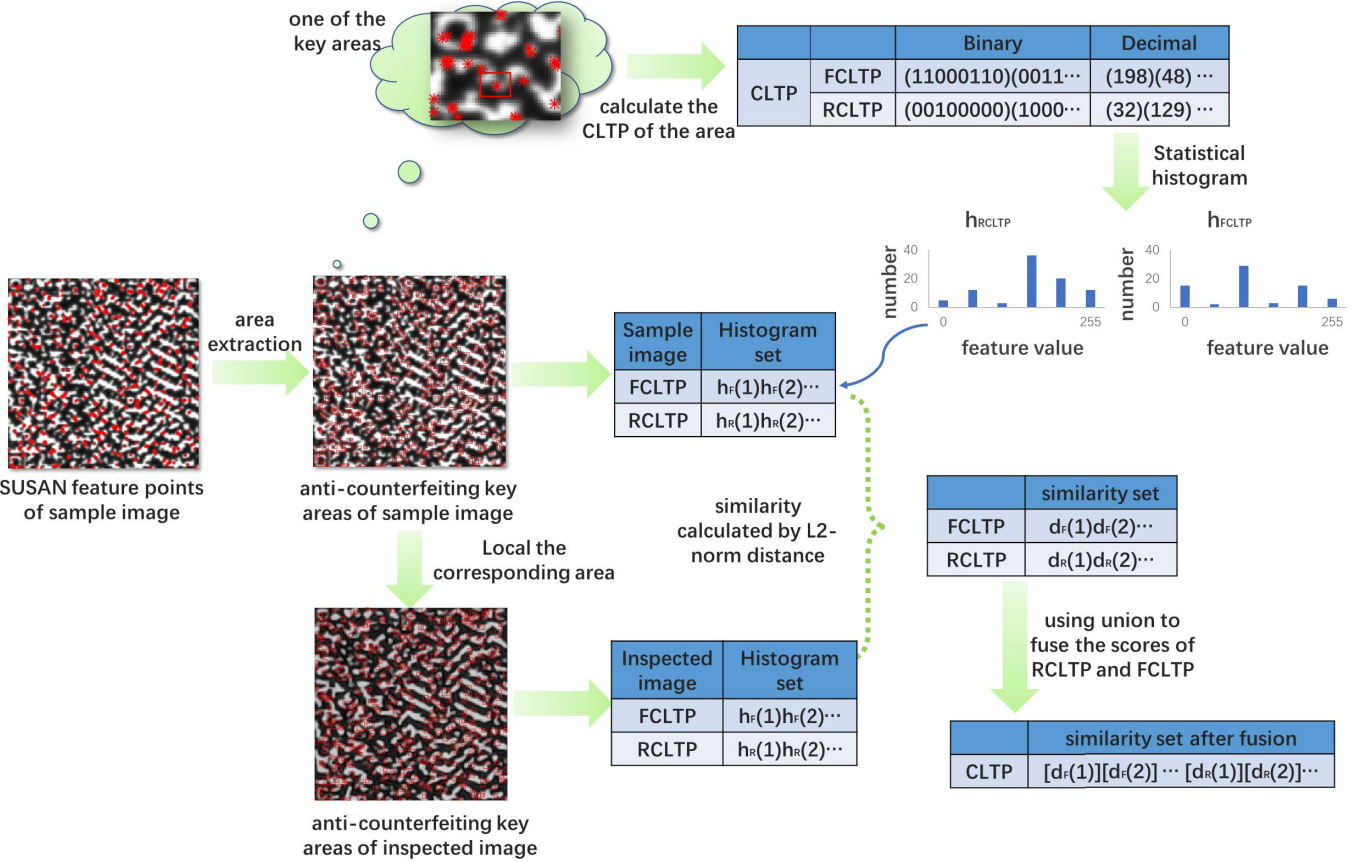


Fig. 10. Flowchart of anti-counterfeiting pattern identification based on CLTP texture features.

TABLE IV  
PERFORMANCE COMPARISON

Anti-counterfeiting algorithm	Precision	Recall	F1-measure
GLCM	83.33%	70.00%	76.09%
WDT	100%	64.00%	78.05%
LBP	100%	80.00%	88.89%
BGC1	100%	88.00%	93.62%
LTP	100%	90.00%	94.74%
LBPcoHDLBP	100%	84.00%	91.30%
MRELBP	100%	90.00%	94.74%
RALBGC	100%	88.00%	93.62%
SDKR	97.00%	91.00%	94.00%
CLTP	100%	99.00%	99.50%

TABLE V  
U-VALUE COMPARISON

Anti-counterfeiting algorithm	U-Value
GLCM	1.594
WDT	15.495
LBP	18.543
BGC1	16.254
LTP	18.643
LBPcoHDLBP	18.752
MRELBP	18.543
RALBGC	16.031
CLTP	19.388

image of the anti-counterfeiting pattern, and the size is normalized to  $256 \times 256$ . In addition, the key point areas of the anti-counterfeiting pattern are extracted(except for SDKR), and the similarity is determined by the L2 norm distance. The performance of the texture descriptors is evaluated using three aspects: the precision and recall rate, the stability and the time consumption.

1) *Precision Rate and Recall Rate:* A simple threshold method is directly used for authenticity identification after the calculation of the similarity. The precision should be as high as possible to ensure that the forged anti-counterfeiting pattern is not judged as a real anti-counterfeiting pattern in

actual use. Table IV summarizes the results of the experiment comparing different texture features and preprocessing using the average precision and recall rates of all data sets. Since forged products are generally not allowed to be judged as real in practical applications, we try to control the Precision rate at 100%. The table shows that in terms of precision and recall rate, in the ranking of the test descriptors, the best method is the CLTP with a 100% average precision and a 99% recall rate, which are better than those of other texture features.

The F1-measure are defined as follows:

$$F1 = 2 * (Precision * Recall) / (Precision + Recall) \quad (24)$$

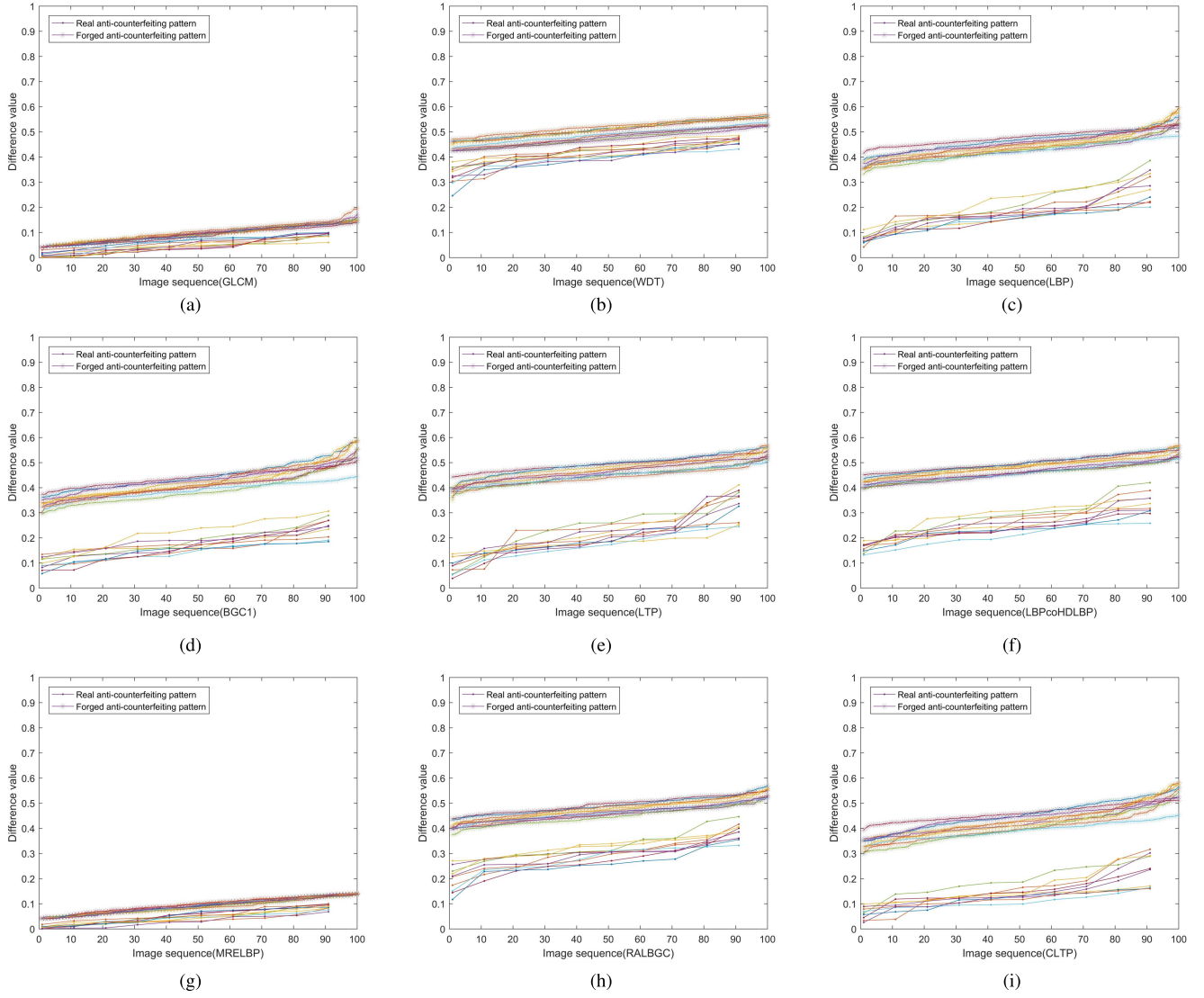


Fig. 11. Scatter diagram of the difference values(the entire image).

2) *Stability*: In the anti-counterfeiting pattern identification process, it is usually expected that the more similar the real anti-counterfeiting image is to the sample image, the greater the differences from the forged anti-counterfeiting images. Therefore, the stability of texture features can be judged by the difference between the similarity distance of the real anti-counterfeiting image and the forged anti-counterfeiting image. To more comprehensively reflect the stability of the features, we separately count the distance differences from the global image and local key areas. Because the key areas extraction method of SDKR is different from other algorithms, it can not be effectively compared, so fig.11 depicts the normalized similarity average distances of the 9 texture features in the entire image dataset in the form of a scatter plot. The asterisk in the figure is the forged anti-counterfeiting pattern, and the real point is the real anti-counterfeiting pattern. The y-coordinate is the normalized number of different anti-counterfeiting key areas in each image, and the x-coordinate is the inspected image sequence. The same color

curve is the same group of image data (including real and forged), and each curve is sorted from small to large according to difference value. Due to the excessive amount of test data, we list the test results of 10 sets of data. Fig.12 depicts the normalized similarity average distances of the 9 texture features in all anti-counterfeiting key areas, where y coordinate is the normalized difference distance of the feature value of each anti-counterfeiting key area, and the x-coordinate is the anti-counterfeiting key areas sequence of the all inspected images. The same color curve is the all key areas of the same group of image data (including real and forged), and each curve is sorted from small to large according to difference value.

Generally, the larger the mean difference between two types of data, the easier it is to distinguish the data; and the smaller the data variance is, the smaller the volatility, and the less likely it is that a pattern will be misjudged. Therefore, a measurable method is needed to judge the stability of each texture feature algorithm. The Mann-Whitney U test is a statistical

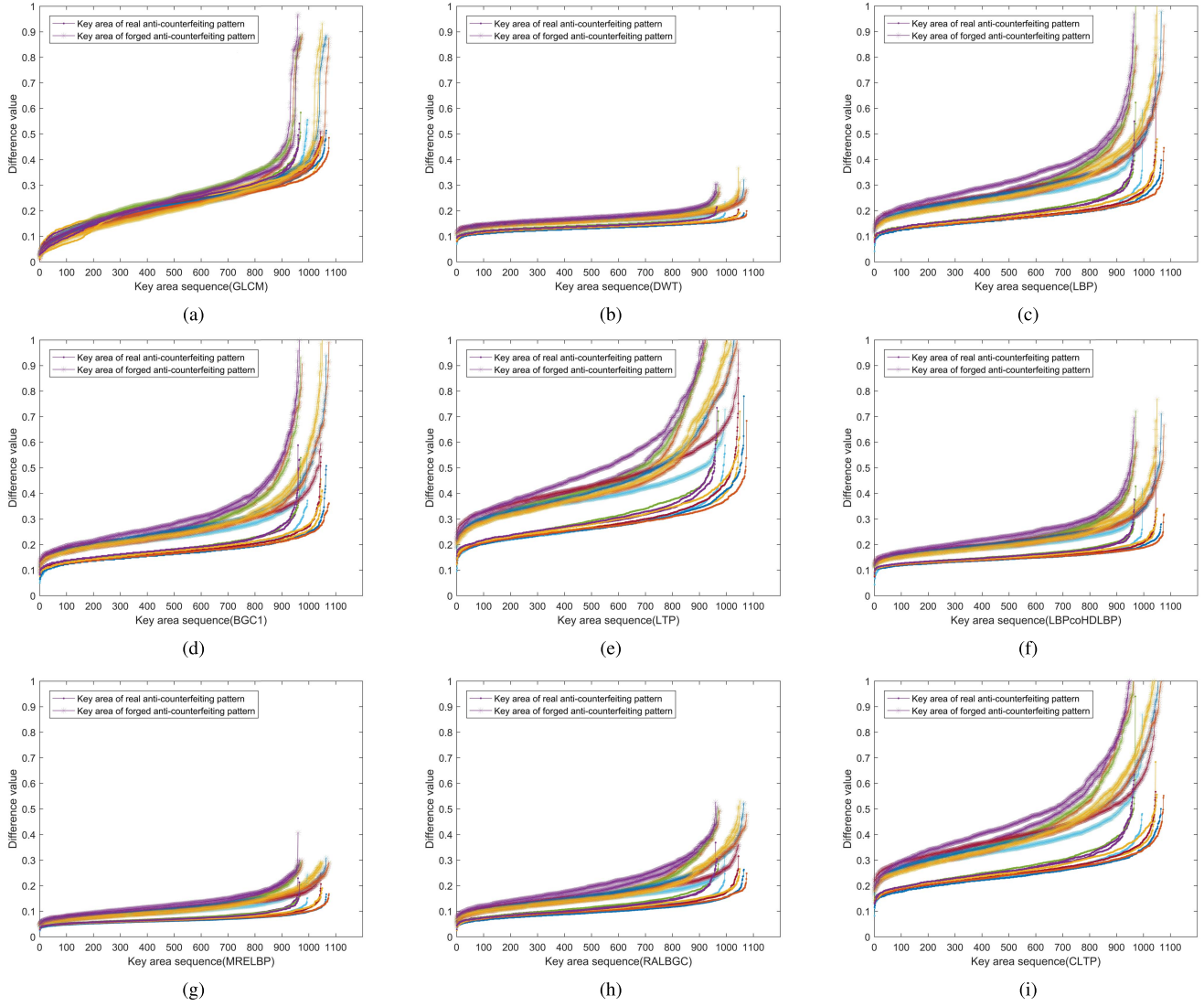


Fig. 12. Scatter diagram of the difference values(the anti-counterfeiting key areas).

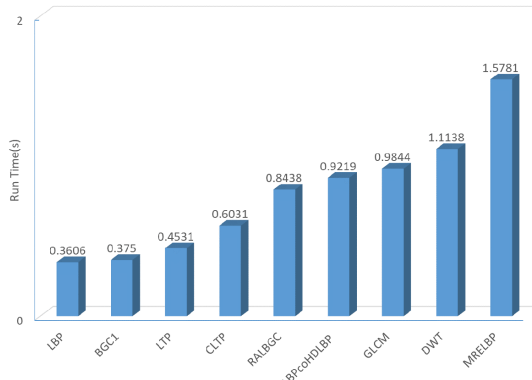


Fig. 13. Running time of each texture feature.

method based on variable ranking without samples conforming to a normal distribution or sample variance alignment. This nonparametric hypothesis test method can assess whether there is a significant difference between two observations. Table V demonstrates the similarity average distances on all

data of 9 kinds of texture features in anti-counterfeiting key areas. The test statistics for the similarity distance results of the real anti-counterfeiting image and that of the forged anti-counterfeiting image are calculated by the Mann-Whitney U test. Generally, the larger the  $U$  value is, the greater the mean difference and the smaller the variance. It can be seen from the results that the CLTP descriptor proposed in this paper is obviously the best method to execute to obtain the maximum difference with the best performance stability.

$$U = \frac{|u_1 - u_2|}{\sqrt{\frac{\sigma_1^2}{n} + \frac{\sigma_2^2}{n}}} \quad (25)$$

where  $u_1$  and  $u_2$  are the mean values of the real and forged anti-counterfeiting images,  $\sigma_1$  and  $\sigma_2$  are the standard deviations of the real and forged anti-counterfeiting images.

3) *Running Time*: Fig.13 displays the running time (in seconds) of each texture feature, including the feature extraction and similarity calculation times of all anti-counterfeiting key areas in the experiment. It can be seen that although the

CLTP method takes 1.67 more time than the traditional LBP, the extra time consumed is worthwhile due to the greatly improved precision rate. Therefore, the CLTP in this paper can greatly improve the precision and stability of texture feature performance at the expense of certain running time and better satisfy the actual needs of anti-counterfeiting identification.

## VII. CONCLUSION

A new texture feature for anti-counterfeiting identification is proposed in this paper. The prominent feature of the descriptor is a coding and recombination strategy. It redefines the CLTP coding strategy by using the relationship between the center and neighborhood and redefines the recombination strategy by using the structural form of the element gradient. Therefore, the ability of the CLTP to identify the details of inkjet printing random features for anti-counterfeiting identification is improved. We test the performance of the CLTP through a series of extensive experiments on an anti-counterfeiting label data set, and the results prove that the CLTP is superior to the latest descriptors on these data set, ensuring the credibility, stability and discrimination of anti-counterfeiting identification. Although it consumes more time than the traditional LBP, it still can satisfy the real-time requirements of practical applications.

Further work may include increasing the coding content and optimizing various parameters related to the method (such as using area blocking and other distance measures) to further enhance the performance of the proposed CLTP in anti-counterfeiting identification scenarios. We can also explore the performance of the CLTP in other recognition scenarios.

## REFERENCES

- [1] A. B. Centeno, O. R. Terrades, J. L. Canet, and C. C. Morales, "Identity document and banknote security forensics: A survey," 2019, *arXiv:1910.08993*.
- [2] Z. Zheng, "A system for identifying an anti-counterfeiting pattern based on the statistical difference in key image regions," *Expert Syst. Appl.*, vol. 183, Nov. 2021, Art. no. 115410.
- [3] J. Gebhardt, M. Goldstein, F. Shafait, and A. Dengel, "Document authentication using printing technique features and unsupervised anomaly detection," in *Proc. 12th Int. Conf. Document Anal. Recognit.*, Aug. 2013, pp. 479–483.
- [4] S. Shang, N. Memon, and X. Kong, "Detecting documents forged by printing and copying," *EURASIP J. Adv. Signal Process.*, vol. 2014, no. 1, pp. 1–13, Dec. 2014.
- [5] M. Umadevi, A. Agarwal, and R. Rao, "Printed text characterization for identifying print technology using expectation maximization algorithm," in *Proc. 5th Int. Conf. Multi-Disciplinary Trends Artif. Intell.*, 2011, pp. 201–212.
- [6] Y. Akao, A. Yamamoto, and Y. Higashikawa, "Improvement of inkjet printer spur gear teeth number estimation by fixing the order in maximum entropy spectral analysis," in *Proc. 4th Int. Workshop Comput. Forensics*, 2010, pp. 101–113.
- [7] S. Elkasrawi and F. Shafait, "Printer identification using supervised learning for document forgery detection," in *Proc. 11th IAPR Int. Workshop Document Anal. Syst.*, Apr. 2014, pp. 146–150.
- [8] H. Wu, X. Kong, and S. Shang, "A printer forensics method using halftone dot arrangement model," in *Proc. IEEE China Summit Int. Conf. Signal Inf. Process. (ChinaSIP)*, Jul. 2015, pp. 861–865.
- [9] Z. Yu *et al.*, "Searching central difference convolutional networks for face anti-spoofing," in *Proc. IEEE/CVF Conf. Comput. Vis. Pattern Recognit. (CVPR)*, Jun. 2020, pp. 5294–5304.
- [10] A. Parkin and O. Grinchuk, "Recognizing multi-modal face spoofing with face recognition networks," in *Proc. IEEE/CVF Conf. Comput. Vis. Pattern Recognit. Workshops (CVPRW)*, Jun. 2019, pp. 1617–1623.
- [11] T. Q. Nguyen, Y. Delignon, L. Chagas, and F. Septier, "Printer identification from micro-metric scale printing," in *Proc. IEEE Int. Conf. Acoust., Speech Signal Process. (ICASSP)*, May 2014, pp. 6236–6239.
- [12] D. G. Kim and H. K. Lee, "Color laser printer identification using photographed halftone images," in *Proc. 22nd Eur. Signal Process. Conf.*, 2014, pp. 795–799.
- [13] D. G. Kim and H.-K. Lee, "Colour laser printer identification using halftone texture fingerprint," *Electron. Lett.*, vol. 51, no. 13, pp. 981–983, Jun. 2015.
- [14] Q. Zhou, Y. Yan, T. Fang, X. Luo, and Q. Chen, "Text-independent printer identification based on texture synthesis," *Multimedia Tools Appl.*, vol. 75, no. 10, pp. 5557–5580, May 2016.
- [15] A. Ferreira, L. C. Navarro, G. Pinheiro, J. A. dos Santos, and A. Rocha, "Laser printer attribution: Exploring new features and beyond," *Forensic Sci. Int.*, vol. 247, pp. 105–125, Feb. 2015.
- [16] A. Ferreira *et al.*, "Data-driven feature characterization techniques for laser printer attribution," *IEEE Trans. Inf. Forensics Security*, vol. 12, no. 8, pp. 1860–1873, Aug. 2017.
- [17] L. C. Navarro, A. K. Navarro, A. Rocha, and R. Dahab, "Connecting the dots: Toward accountable machine-learning printer attribution methods," *J. Vis. Commun. Image Represent.*, vol. 53, pp. 257–272, May 2018.
- [18] M. J. Tsai, J. S. Yin, I. Yuadi, and J. Liu, "Digital forensics of printed source identification for Chinese characters," *Multimedia Tools Appl.*, vol. 73, no. 3, pp. 2129–2155, Dec. 2014.
- [19] M.-J. Tsai, C.-L. Hsu, J.-S. Yin, and I. Yuadi, "Japanese character based printed source identification," in *Proc. IEEE Int. Symp. Circuits Syst. (ISCAS)*, May 2015, pp. 2800–2803.
- [20] S. Joshi and N. Khanna, "Single classifier-based passive system for source printer classification using local texture features," *IEEE Trans. Inf. Forensics Security*, vol. 13, no. 7, pp. 1603–1614, Jul. 2018.
- [21] J. Sharad and N. Khanna, "Source printer classification using printer specific local texture descriptor," *IEEE Trans. Inf. Forensics Security*, vol. 15, pp. 160–171, 2019.
- [22] C. Chen, M. Li, A. Ferreira, J. Huang, and R. Cai, "A copy-proof scheme based on the spectral and spatial barcoding channel models," *IEEE Trans. Inf. Forensics Security*, vol. 15, pp. 1056–1071, 2020.
- [23] J. Picard, P. Landry, and M. Bolay, "Counterfeit detection with QR codes," in *Proc. 21st ACM Symp. Document Eng.*, Aug. 2021, pp. 1–4.
- [24] Y. C. Li, "Automatic identification algorithm of texture anti-counterfeiting tag base on transform domain," M.S. thesis, Hainan Univ., 2015.
- [25] Y. Zhang, "A research of automatic identification algorithm of authentic work anti-counterfeiting label," M.S. thesis, Hainan Univ., 2017.
- [26] T. Ojala, M. Pietikainen, and D. Harwood, "Performance evaluation of texture measures with classification based on Kullback discrimination of distributions," in *Proc. 12th Int. Conf. Pattern Recognit.*, 1994, pp. 582–585.
- [27] A. Fernández, M. X. Álvarez, and F. Bianconi, "Image classification with binary gradient contours," *Opt. Lasers Eng.*, vol. 49, nos. 9–10, pp. 1177–1184, Sep. 2011.
- [28] X. Tan and B. Triggs, "Enhanced local texture feature sets for face recognition under difficult lighting conditions," *IEEE Trans. Image Process.*, vol. 19, no. 6, pp. 1635–1650, Oct. 2010.
- [29] Z. H. Zheng *et al.*, "Feedback unilateral grid-based clustering feature matching for remote sensing image registration," *Remote Sens.*, vol. 11, no. 12, pp. 1418–1429, 2019.
- [30] J. Ma, J. Zhao, J. Jiang, H. Zhou, and X. Guo, "Locality preserving matching," *Int. J. Comput. Vis.*, vol. 127, no. 5, pp. 512–531, 2019.
- [31] S. M. Smith and J. M. Brady, "SUSAN-a new approach to low level image processing," *Int. J. Comput. Vis.*, vol. 23, no. 1, pp. 45–78, 1997.
- [32] F. Yuan, X. Xia, and J. Shi, "Mixed co-occurrence of local binary patterns and Hamming-distance-based local binary patterns," *Inf. Sci.*, vol. 460–461, pp. 202–222, Sep. 2018.
- [33] L. Liu, S. Lao, P. W. Fieguth, Y. Guo, X. Wang, and M. Pietikäinen, "Median robust extended local binary pattern for texture classification," *IEEE Trans. Image Process.*, vol. 25, no. 3, pp. 1368–1381, Mar. 2016.
- [34] I. E. Khadri, M. Kas, Y. El Merabet, Y. Ruichek, and R. Touahni, "Repulsive-and-attractive local binary gradient contours: New and efficient feature descriptors for texture classification," *Inf. Sci.*, vol. 467, pp. 634–653, Oct. 2018.